2016-08

Monitoring abiotic degradation in sinking versus suspended Arctic sea ice algae during a spring ice melt using specific lipid oxidation tracers

Rontani, J-F

10.1016/j.orggeochem.2016.05.016
Organic Geochemistry
Elsevier BV

Monitoring abiotic degradation in sinking versus suspended Arctic sea ice algae during a spring ice melt using specific lipid oxidation tracers

Jean-François Rontani [a*], Simon T. Belt [b], Thomas A. Brown [b], Rémi Amiraux [a], Michel Gosselin [c], Frédéric Vaultier [a], Christopher J. Mundy [d]

[a] *Aix Marseille Université, Université de Toulon, CNRS/INSU/IRD, Mediterranean Institute of Oceanography (MIO) UM 110, 13288, Marseille, France*

[b] *Biogeochemistry Research Centre, School of Geography, Earth and Environmental Sciences, University of Plymouth, Drake Circus, Plymouth, Devon PL4 8AA, UK*

[c] *Institut des sciences de la mer (ISMER), 310 Allée des Ursulines, Université du Québec à Rimouski, Rimouski, Québec G5L 3A1, Canada*

[d] *Centre for Earth Observation Science (CEOS), Department of Environment and Geography, CHR Faculty of Environment, Earth and Resources, University of Manitoba, Winnipeg, Manitoba R3T 2N2, Canada*

* Corresponding author. Tel.: +33-4-86-09-06-02; fax: +33-4-91-82-96-41.

ABSTRACT

The abiotic degradation state of sea ice algae released during a late spring ice melt process was determined by sampling the underlying waters and measuring certain well-known algal lipids and their oxidation products, including those derived from epi-brassicasterol, 24-methylenecholesterol, palmitoleic acid and the phytyl side-chain of chlorophyll. More specifically, parent lipids and some of their oxidation products were quantified in suspended (collected by filtration) and sinking (collected with sediment traps at 5 and 30 m) particles from Resolute Passage (Canada) during a period of spring ice melt in 2012 and the outcomes compared with those obtained from related sea ice samples analyzed previously. Our data show that suspended cells in the near surface waters appeared to be only very weakly affected by photooxidative processes, likely indicative of a community of unaggregated living cells with high seeding potential for further growth. In contrast, we attribute the strong photooxidation state of the organic matter in the sediment traps deployed at 5 m to the presence of senescent and somewhat aggregated sea ice algae that descended only relatively slowly within the euphotic zone, and was thus susceptible to photochemical degradation. On the other hand, the increased abiotic preservation of the sinking material collected in the sediment traps deployed at 30 m, likely reflected more highly aggregated senescent sea ice algae that settled sufficiently rapidly out of the euphotic zone to avoid significant photooxidation. This better-preserved sinking material in the deeper sediment traps may therefore contribute more strongly to the underlying sediments. A three-component conceptual scheme summarizing the abiotic behavior of Arctic sea ice algae in underlying waters is proposed.

Keywords: Sea ice algae; Suspended and sinking particles; Lipid oxidation products; Photooxidation; Preservation; Aggregation.

1. Introduction

Sea ice is a key parameter in controlling global climate (Ferrari et al., 2014) and within the polar regions, in particular, due to its influence on surface albedo (Hartmann, 1994; Curry et al., 1995) and by providing a physical barrier that limits the exchange of heat, moisture and gases between the ocean and the atmosphere. The extent, nature and seasonality of sea ice also impacts on polar marine ecosystems across all trophic levels, not least at the base of the food web, where it provides a physical environment suitable for the development and growth of ice algal communities and a range of heterotrophic eukaryotes (Różańska et al., 2009; Caron and Gast, 2010). The bottom (ca. 10 cm) sections of annually formed Arctic sea ice comprises an interstitial community of ice crystals, brine pockets and a network of channels and capillaries that provide a host for the growth of an adapted community of microalgae (Horner et al., 1992; Arrigo et al., 2010) that represent a critical food source for ice-associated and pelagic herbivorous protists (Michel et al., 2002) and metazoans (Nozais et al., 2001). Such is the importance of this community, it has been estimated that the contribution of sea ice algae to total primary production is ca. 3–25% on Arctic shelves (e.g., Legendre et al., 1992) and as much as 57% in the central Arctic Ocean (Gosselin et al., 1997). During the early stages of ice melt, and prior to ice break-up, ice algae are released from bottom ice into the water column, where they can make a significant contribution to the cycling of organic carbon throughout the Arctic (e.g., Michel et al., 2006). In addition to the production of photosynthetic pigments (e.g., chlorophyll) and storage lipids (e.g., fatty acids) common to all microalgae, sea ice algae also produce extracellular polymeric substances (EPS), which play multiple roles in the entrapment, retention and survival of these organisms within the sea ice matrix (Ewert and Deming, 2013). Further, the production of EPS not only facilitates the attachment of algae to the ice substrate itself, but also the formation of microaggregates of

algal cells that can remain intact after ice melt (Riebesell et al., 1991). As a result, the sedimentation of ice algae can be enhanced relative to otherwise isolated cells that tend to remain in suspension or, at least, have longer residence times in near surface waters.

Elucidation of the fate of algal material in the water column during and after sea ice melt in the Arctic constitutes a very important challenge (Tedesco et al., 2012; Vancoppenolle et al., 2013). It is generally considered that a part (until now not estimated) of this strong pulse of particulate organic matter (POM), which is not degraded by bacteria or grazed by heterotrophs such as zooplankton during its descent to the seafloor, may be stored in sediments (Fortier et al., 2002; Renaud et al., 2007). However, the integrity of the OM in such settings remains largely unexamined.

Although less widely studied than its biologically mediated (heterotrophic) counterpart, photooxidative degradation is now known to play a significant role in the fate of POM in the open ocean (Rontani, 2008; Estapa and Mayer, 2010), with photosensitization playing an important role in the photodegradation of algal detritus (Nelson, 1993; Mayer et al., 2009). Due to the presence of chlorophyll and pheopigments, which are well-known sensitizers of Type II photooxidation processes (i.e. involving singlet oxygen ($^1O_2$); Kessel and Smith, 1989), and the longer lifetime of $^1O_2$ in lipid-rich membranes compared to aqueous solution (Suwa et al., 1977), Type II photosensitized oxidation processes act intensively in senescent algae (Rontani, 2012). Such processes afford hydroperoxides, which, after subsequent homolytic cleavage, are responsible for the induction of autoxidation (free radical-induced oxidation) processes (Girotti, 1998; Rontani et al., 2003). It has also been demonstrated that Type II photosensitized oxidation appears to be particularly efficient in natural samples in the Arctic (Rontani et al., 2012) and also in senescent phytoplanktonic cells under in vitro conditions, despite low temperatures and irradiances (Amiraux et al., 2016). This apparent paradox has been attributed to a combination of the relative preservation of the

sensitizer (chlorophyll) at low irradiances, which permits a longer production time for $^1O_2$, and the slower diffusion rate of $^1O_2$ through the cell membranes at low temperatures (Ehrenberg et al., 1998), thus favoring the intra-cellular involvement of Type II photosensitized reactions. Potentially, therefore, the low irradiance and low temperature conditions that are characteristic of the under-ice environment in the Arctic could strongly favor the photodegradation of algae released by melting sea ice. However, it is also important to note that these photodegradation processes are also strongly dependent on both the residence time of cells within the euphotic layer (Zafiriou et al., 1984; Mayer et al., 2009) and the physiological state of the phytoplanktonic cells themselves (Merzlyak and Hendry, 1994; Nelson, 1993). Indeed, $^1O_2$ production can exceed the quenching capacities of the photoprotective system (and thus induce cell damage) only when the photosynthetic pathways are not operative, as is the case for senescent or highly stressed cells (Nelson, 1993). Interestingly, Ligowski et al. (1992) previously failed to detect photosynthesis in diatoms from brash ice after ice melting, while Ralph et al. (2007) concluded that sea ice algal cells are more susceptible to photosynthetic stress during ice melt compared to their incorporation into the ice matrix during the freezing process. The involvement of photochemical damage in sea ice algal material released during ice melt is thus very likely. However, by recording rates of oxygen production and consumption between aggregated and dispersed ice algae, Riebesell et al. (1991) suggested that metabolically less active ice algae tend to be concentrated in aggregates, while growing cells are more likely to remain unaggregated. As a result, the organic content of suspended and sinking sea ice material might be expected to exhibit contrasting photo-oxidation states.

The purpose of this study, therefore, was to apply a suite of specific lipid oxidation tracers (Fig. 1) to monitor the degradation of sea ice algae in suspended (collected by filtration) and sinking (collected with sediment traps) particles from Resolute Passage

(Canada) during a period of spring ice melt (but continuous sea ice cover), and for which the corresponding sea ice algal lipid composition and degradation state had previously been established (Rontani et al., 2014). In particular, we aimed to compare the degradation states of suspended and sinking OM during the early stages of ice melt, and to identify how the sensitivity of the released sea ice algal-derived OM towards photodegradation was dependent on the aggregation state of the algal cells.

With the specific aim of characterizing the abiotic (photo-oxidation) degradation state of sea ice algal material in the water column, we focused our analyses on chlorophyll and a range of lipids along with some of their degradation products (Fig. 1). Such lipids included certain diatom-derived highly branched isoprenoid (HBI) alkenes (including IP_{25}, which is made uniquely by sea ice diatoms, Belt et al., 2007; 2013; Brown et al., 2014), the mono-unsaturated fatty acid $C_{16:1\omega7}$ (palmitoleic acid; the dominant monounsaturated fatty acid of sea-ice algae, Fahl and Kattner, 1993; Leu et al., 2010), together with the Δ^5-sterols 24-methylcholesta-5,22*E*-dien-3β-ol (termed epi-brassicasterol here since diatoms synthesize the 24α-isomer) and 24-methylcholesta-5,24(28)-dien-3β-ol (24-methylenecholesterol) (generally considered to be specific to phytoplankton, Volkman, 1986; 2003). The analysis of other common lipids such as $C_{18:1\omega9}$ (oleic acid), cholest-5-en-3β-ol (cholesterol), 24-methylcholest-5-en-3β-ol (campesterol) and 24-ethylcholest-5-en-3β-ol (sitosterol) was not included in this study as they are not sufficiently specific to sea ice algal or phytoplankton sources.

2. Experimental

2.1. Study location and sample collection

This study was conducted in 2012 at a landfast ice station (74° 43.613′ N, 95° 33.496′ W; water column depth: 90 m) located between Griffith Island and Sheringham Point

(Cornwallis Island) in Resolute Passage, Nunavut, Canada. The thickness of the first-year ice was ca. 1.27 m at the beginning of the sampling period (Galindo et al., 2015). From 22 May to 20 June 2012, suspended particulate matter (SPM) samples were collected at 2, 5 and 10 m with 5 l Niskin bottles. From 18 May to 23 June, sediment trap samples were collected with two Hydro-Bios multi-sediment traps MS12 that were deployed at 5 m and 30 m from the undersurface of the ice. The interceptor traps, fixed to a tripod on the sea ice, were made of polyvinyl chloride (PVC) with an internal diameter of 13 cm and an aspect ratio (height:diameter) of 4. Each trap was fitted with a plastic baffle mounted in the opening, to prevent the entrance of larger organisms. In the receiving cups, a 5% buffered formalin-seawater solution was used as a preservative (Hargrave et al., 2002). The trap rotation interval was every three days. Upon recovery, samples were stored at 4 °C in the dark until further analysis. Sub-samples for lipid analysis were filtered onto Whatman GF/F 47 mm filters, kept frozen at –80 °C, then lyophilized before sending them to the Plymouth laboratory. Photochemically Active Radiation (PAR) at 5 and 30 m underneath the ice was estimated from vertical profiles made with a scalar PAR sensor (Biospherical QSP-2300) mounted on a Sea-Bird SBE 19plus V2 conductivity-temperature-depth (CTD) probe.

Although the presence of formalin would have prevented biotic degradation, the same may not have been entirely the case for abiotic degradation processes in the sediment traps, with some autoxidation possibly having taking place, even in the absence of light. In contrast, the shading effect of the trap material on the receiving flasks and the thickness of their plastic layer, likely minimized or even prevented photodegradation processes entirely, such that these are considered to have been negligible. Overall, the intensity of autoxidation and photooxidation processes, which did not increase significantly with sampling time, suggest that abiotic processes were not significant during the time series.

175 *2.2. Sample treatment*

176 Contents of HBIs and oxidation products of other lipids (Δ^5-sterols, fatty acids and
177 chlorophyll phytyl side-chain) were determined separately on individual samples (filters). The
178 treatment of filters for HBI analysis (alkaline hydrolysis and purification by open column
179 chromatography) and lipid oxidation product measurement ($NaBH_4$ reduction and alkaline
180 hydrolysis) was performed as described previously (Brown et al., 2011; Rontani et al., 2014).
181
182 *2.3. Derivatization*

183 For extracts containing hydroxyl functions (i.e. sterols, fatty acids and oxidation
184 products), samples were derivatized by dissolving them in 300 µl of a mixture of pyridine and
185 BSTFA (Supelco; 2:1, v/v) and silylated (1 h) at 50 °C. After evaporation to dryness under a
186 stream of N_2, the derivatized residue was dissolved in a mixture of hexane and BSTFA (to
187 avoid desilylation) and analyzed by GC–MS–MS or GC–QTOF.
188
189 *2.4. Gas chromatography/electron impact mass spectrometry (GC–EIMS)*

190 HBIs were analyzed and quantified by GC–EIMS in Selective Ion Monitoring (SIM)
191 mode (*m/z* 350.3, 348.3, 346.3, limit of detection = 1 ng/l) using an Agilent 7890A gas
192 chromatograph coupled to an Agilent 5975c quadrupole mass spectrometer (GC–MS; HP5ms;
193 Belt et al., 2012). Comparison of retention indices and mass spectra of HBIs in sample
194 extracts to those obtained from purified standards permitted unambiguous identification.
195 Quantification of HBIs was achieved by comparison of SIM peak areas with those of the
196 internal standard (9-octylheptadec-8-ene; 2 ng) and normalised to individual response factors
197 (Belt et al., 2012) and sample volumes.
198
199 *2.5. Gas chromatography–electron ionization tandem mass spectrometry (GC–MS–MS)*

Fatty acids, phytol and their oxidation products were identified and quantified using an Agilent 7890A/7000A tandem quadrupole gas chromatograph system (Agilent Technologies, Parc Technopolis - ZA Courtaboeuf, Les Ulis, France). A cross-linked 5% phenyl-methylpolysiloxane (Agilent; HP-5MS) (30 m × 0.25 mm, 0.25 µm film thickness) capillary column was employed. Analyses were performed with a multi-mode injector operating in splitless mode (with 0.5 min splitless period) set at 270 °C and the oven temperature programmed from 70 °C to 130 °C at 20°C/min, then to 250 °C at 5 °C/min and then to 300 °C at 3 °C/min. The pressure of the carrier gas (He) was maintained at 0.69×10^5 Pa until the end of the temperature program and then programmed from 0.69×10^5 Pa to 1.49×10^5 Pa at 0.04×10^5 Pa/min. The following mass spectrometric conditions were employed: electron energy, 70 eV; source temperature, 230 °C; quadrupole 1 temperature, 150 °C; quadrupole 2 temperature, 150 °C; collision gas (N_2) flow, 1.5 ml/min; quench gas (He) flow, 2.25 ml/min; mass range, 50–700 Da; cycle time, 313 ms. Quantification of analytes was carried out with external standards in Multiple Reaction Monitoring (MRM) mode. MRM transitions were selected after CID (Collision Induced Dissociation) analyses of all the precursor ions corresponding to the more intense fragment ions observed in EI mass spectra of the compounds of interest.

2.6. Gas chromatography–electron ionization quadrupole time of flight mass spectrometry (GC–QTOF)

Δ^5-sterols and their oxidation products were identified and quantified with an Agilent 7890B/7200 GC–QTOF System (Agilent Technologies, Parc Technopolis - ZA Courtaboeuf, Les Ulis, France). A cross-linked 5% phenyl-methylpolysiloxane (Agilent; HP-5MS ultra inert) (30 m × 0.25 mm, 0.25 µm film thickness) capillary column was employed. Analyses were performed with an injector operating in pulsed splitless set at 280 °C and the oven

temperature programmed from 70 °C to 130 °C at 20 °C/min, then to 250 °C at 5 °C/min and then to 300 °C at 3 °C/min. The pressure of the carrier gas (He) was maintained at 0.69×10^5 Pa until the end of the temperature program. Instrument temperatures were 300 °C for transfer line and 230 °C for the ion source. Accurate mass spectra were recorded across the range *m*/*z* 50–700 at 4 GHz. The QTOF MS instrument provided a typical resolution ranging from 8009 to 12252 from *m*/*z* 68.9955 to 501.9706. Perfluorotributylamine (PFTBA) was utilized for daily MS calibration. Identification and quantification were carried out with external standards in Time of Flight (TOF) mode.

2.7. Chlorophyll analyses

Duplicate sub-samples were filtered through 25 mm Whatman GF/F filters. Chlorophyll *a* retained on the filters was measured using a 10-005R Turner Designs fluorometer, after extraction in 90% acetone for 18 h at 4 °C in the dark (acidification method of Parsons et al. (1984)). The fluorometer was calibrated with a commercially available chlorophyll *a* standard (from *Anacystis nidulans*, Sigma).

2.8. Lipid oxidation products employed as tracers

2.8.1. Chlorophyll a

Although it has been shown that the visible light-dependent degradation rate of the tetrapyrrole ring in chlorophyll *a* (chl *a*) is three to five times higher than that of the phytyl side-chain (Cuny et al., 1999; Christodoulou et al., 2010), no specific and stable photodegradation products of the former have been identified in the literature. In contrast, Type II photosensitized oxidation (i.e. involving $^1O_2$) of the phytyl side-chain leads to the well-known production of 2-hydroperoxy-3-methylidene-7,11,15-trimethylhexadecan-1-ol which, after $NaBH_4$ reduction, can be quantified as 3-methylidene-7,11,15-

trimethylhexadecan-1,2-diol (phytyldiol) (Rontani et al., 1994) (Fig. 1). Indeed, phytyldiol is ubiquitous in the marine environment and constitutes a stable and specific tracer for the photodegradation of the chlorophyll phytyl side-chain (Rontani et al., 1996; Cuny and Rontani, 1999). Further, the molar ratio phytyldiol:phytol (Chlorophyll Phytyl side-chain Photodegradation Index, CPPI) has been proposed to estimate the extent of photodegradation of chlorophylls possessing a phytyl side-chain in natural marine samples through use of the empirical equation: chlorophyll photodegradation % = $(1 - [\mathrm{CPPI} + 1]^{-18.5}) \times 100$ (Cuny et al., 1999). The chlorophyll phytyl side-chain is also sensitive to free radical oxidation (autoxidation) reactions. *Z*- and *E*- 3,7,11,15-tetramethylhexadec-3-ene-1,2-diols and 3,7,11,15-tetramethylhexadec-2-ene-1,4-diols have been proposed previously as tracers of these processes (Rontani and Aubert, 2005) (Fig. 1).

2.8.2. HBI alkenes

The biomarker 2,6,10,14-tetramethyl-7-(3-methylpent-4-enyl)-pentadecane (IP_{25}; 'Ice Proxy with 25 carbon atoms'; Belt et al., 2007) is produced by certain Arctic sea ice diatoms during the spring sea ice algal bloom (March–May) (Brown et al., 2011; 2014; Belt et al., 2013) and has been used in a number of studies to provide proxy-based evidence for palaeo sea ice occurrence for several Arctic regions (Belt and Müller, 2013) and as a tracer for the incorporation of sea ice algal OM into Arctic food webs (Brown and Belt, 2012a; 2012b). Sea ice diatoms also produce smaller quantities of HBI trienes with tri-substituted double bonds such as 2,6,10,14-tetramethyl-7-(3-methylpenta-1,4-dienyl)-pentadeca-7(20*E*),9*E/Z*-dienes (Belt et al., 2007; Brown, 2011). Due to the presence of two tri-substituted double bonds that are very reactive towards $^1O_2$ and a *bis*-allylic carbon atom (where hydrogen abstraction is highly favored), these specific HBI trienes are particularly sensitive to photooxidation (Rontani et al., 2011) and autoxidation (Rontani et al., 2014). However, it is not possible to

quantify their photoproducts due to further (and rapid) oxidation of the primary products (Rontani et al., 2014). In contrast, the mono-unsaturated HBI IP_{25}, only possesses a single low reactivity methylidene group, and is thus essentially unaffected by these two abiotic degradation processes. As a consequence, the ratio between these two HBI lipids ($C_{25:3}$(*E*)/IP_{25}) constitutes a potentially very useful tool for estimating changes to the degradation state of sea ice algae.

2.8.3. Monounsaturated fatty acids

Autoxidation and photooxidation of monounsaturated fatty acids lead to the formation of oxidation products that are sufficiently stable in the marine environment to act as tracers of abiotic degradation processes (Rontani, 2012). $^1O_2$-mediated photooxidation of palmitoleic acid, for example, produces a mixture of 9- and 10-hydroperoxides with an allylic *trans*-double bond (Frankel et al., 1979), which can subsequently undergo highly stereoselective radical allylic rearrangement to 11-*trans* and 8-*trans* hydroperoxides, respectively (Porter et al., 1995) (Fig. 1). In contrast, autoxidation (free radical-induced oxidation) affords a mixture of 9-*trans*, 10-*trans*, 11-*trans*, 11-*cis*, 8-*trans*, and 8-*cis* hydroperoxides (Frankel, 1998) (Fig. 1). For the current study, therefore, the relative importance of autoxidative and photooxidative degradation of palmitoleic acid was estimated on the basis of the proportion of its specific *cis*-oxidation products and of the water temperature according to the approach described previously by Marchand and Rontani (2001).

2.8.4. Δ^5-sterols

$^1O_2$-mediated photooxidation of Δ^5-sterols produces mainly Δ^6-5α-hydroperoxides with smaller amounts of Δ^4-6α/6β-hydroperoxides (Kulig and Smith, 1973), while their autoxidation yields mainly 7α-and 7β-hydroperoxides and, to a lesser extent, 5α/β,6α/β-

epoxysterols and 3β,5α,6β-trihydroxysterols (Smith, 1981). On the basis of their stabilities and specificities, Δ^4-stera-3β,6α/β-diols (resulting from $NaBH_4$-reduction of Δ^4-6α/6β-hydroperoxides) and 3β,5α,6β-steratriols were previously selected as tracers of Δ^5-sterol photooxidation and autoxidation, respectively (Rontani et al., 2009) (Fig. 1), and the extent of these degradation processes may be estimated using different equations previously proposed by Christodoulou et al. (2009). It may also be noted that, in the case of di-unsaturated sterols, autoxidation estimates are not possible due to the additional attack of the double bond of the lateral chain precluding 3β,5α,6β-steratriol accumulation.

2.8.5. Production of standard oxidation products

Standard oxidation products of monounsaturated fatty acids, chlorophyll phytyl side-chain, and Δ^5-sterols were obtained according to previously described procedures (Rontani and Marchand, 2000; Marchand and Rontani, 2001; Rontani and Aubert, 2005).

3. Results

3.1. SPM samples

The concentration of chl *a* was measured in all the SPM samples and showed a clear increase at 2 m from 30 May to 11 June (Table 1). On the other hand, quantification of phytol and phytyldiol allowed us to show that the photooxidation percentage of chlorophyll in the different SPM samples was relatively low, particularly at 2 m, with values ranging from 0–30% (Fig. 2A). At 5 m and 10 m, the photooxidation percentage reached 50% and 40%, respectively (Fig. 2B and C). In contrast, we failed to detect autoxidation products of chlorophyll phytyl side-chain in any of the SPM samples.

The $C_{25:3}$(*E*)/IP_{25} ratios (g/g) in the SPM from 22 May to 03 June (0.219 ± 0.062, 0.313 ± 0.096 and 0.246 ± 0.059 at 2, 5 and 10 m, respectively) (Table 2) were close to that measured in the corresponding bottom (0–3 cm) sea ice (0.244 ± 0.235 g/g) (Belt et al., 2013).

Within the fatty acids, the SPM was dominated by palmitoleic acid, as expected, with a strong increase in the concentration of all components at 2 m from 30 May to 07 June (Fig. 3A). A general decrease in the concentration of fatty acids could be observed with depth, however (Fig. 3B and C). Quantification of the photo- and autoxidation products of palmitoleic acid confirmed the very weak abiotic degradation state of the material collected at 2 m between 30 May and 7 June (Fig. 4A). Similar trends could also be observed at 5 and 10 m (Fig. 4B and C). Finally, consistent with the profiles of chl *a* and palmitoleic acid, the concentrations of epi-brassicasterol and 24-methylenecholesterol at 2 m increased significantly from 30 May to 07 June (Table 1). However, no photooxidation products of epi-brassicasterol and 24-methylenecholesterol could be detected in any of the SPM samples.

3.2. Sediment trap samples

The fluxes of chl *a* appeared to be very distinct at the two depths investigated (5 and 30 m). Indeed, the flux of chl *a* remained relatively low (< 0.06 mg/m²/d) at 5 m prior to a rapid increase to 0.58 mg/m²/d from 17 June to 23 June (Fig. 5A). In contrast, generally higher fluxes of chl *a* were identified at 30 m, with values ranging from 0.1–0.45 mg/m²/d (Fig. 5C). CPPI-based chlorophyll photooxidation estimates ranged from 40–100% at 5 m during the first part of the time series, before a rapid decrease occurred from 11 June to 23 June (Fig. 5B). In contrast, chlorophyll was only relatively weakly photooxidized at 30 m throughout the sampling period (CPPI values ranging from 5 to 35%) (Fig. 5D). Autoxidation of the chlorophyll phytyl side-chain appeared to be very weak in all of the samples of sinking particles investigated.

348 The mean values of the $C_{25:3}$(*E*)/IP_{25} ratio (g/g) in the sediment traps (0.004 ± 0.008 and
349 0.142 ± 0.051 at 5 and 30 m, respectively) (Table 3) were lower than those for the
350 corresponding sea ice (0.244 ± 0.235) (Belt et al., 2013) and SPM samples (any depth, see
351 earlier values) indicating a high degree of abiotic degradation of material collected at 5 m, yet
352 relative preservation at 30 m. The fluxes of (total) fatty acids (Fig. 6A and B) paralleled those
353 of chl *a* (Fig. 5A and C) at both depths, with substantially increased values towards the end of
354 sampling at 5 m and higher (and more consistent) values at 30 m. In addition, the fatty acid
355 profiles at 30 m exhibited a strong dominance of $C_{16:0}$ (palmitic) and palmitoleic acids (Fig.
356 6B) as observed previously in the corresponding sea ice samples (Rontani et al., 2014). The
357 identification of 8-*trans*, 9-*trans,* 10-*trans* and 11-*trans* allylic hydroxyhexadecenoic acids as
358 the major palmitoleic acid oxidation products indicated that the degradation mainly resulted
359 from the involvement of photooxidative processes, while quantification of the products of
360 palmitoleic acid showed that the extent of oxidation was lower at 30 m (Fig. 7B) compared to
361 5 m (Fig. 7A).

362 Similar degradation trends could also be observed for the two diatom sterols epi-
363 brassicasterol and 24-methylenecholesterol. Thus, only small proportions of oxidation
364 products of epi-brassicasterol and 24-methylenecholesterol were found at 30 m (Fig. 8B and
365 D), while quantification of the same sterols and of their oxidation products at 5 m gave
366 evidence for strongly photodegraded algal material from 02 June to 14 June (Fig. 8A and C).
367 Interestingly, the extent of photo-oxidation of 24-methylenecholesterol was greater than that
368 of epi-brassicasterol, consistent with previous observations made in sea ice (Rontani et al.,
369 2014) and in suspended particles collected in the Beaufort Sea (Rontani et al., 2012). The
370 presence of an under-ice bloom at the end of the time series could also be observed at both
371 depths (Fig. 8).
372

4. Discussion

During the period investigated, sea ice thickness reduced from 127 to 93 cm and snow cover from 16 to 4 cm. As a result of decreased snow cover, the under-ice PAR increased from 5 to 200 µmol photons/m²/s and from 0.5 to 32 µmol photons/m²/s at 5 and 30 m depth, respectively. Under-ice seawater exhibited relatively consistent hydrographic conditions with temperature ranging from –1.4 to –1.8 °C and salinity from 31.5 to 32.4 between 2 and 80 m (Brown et al., 2016).

4.1. SPM samples

The highest concentrations of palmitoleic acid and the two sterols, epi-brassicasterol and 24-methylenecholesterol, observed in the near surface waters (2 m) during the early sampling dates (Fig. 3A, Table 1), is consistent with quantitative estimates of sea ice algae released during the first phase of ice melt representing close to 100% of the total particulate organic carbon (POC) (Brown et al., 2016).

A small (ca. 4 day) lag, however, was observed for peak chl *a* compared to the lipid tracers (Table 1) which we attribute to the likely additional release of cyanobacteria, especially since these autotrophic organisms contain lower proportions of palmitoleic acid compared to diatoms, do not synthesize sterols (Volkman, 2003; 2005) and may comprise up to 7% of the microbial community of Arctic sea ice (Bowman et al., 2012).

With respect to degradation, the efficiency of type II photo-processes upon HBI alkenes and other well-known phytoplanktonic lipids was previously determined in senescent cells of the diatom *Haslea ostrearia* (Rontani et al., 2011) and the following order of reactivity was demonstrated: $C_{25:3}$ HBI > palmitoleic acid or chlorophyll phytyl side-chain > Δ^5-sterols). Although a similar trend in photodegradation might, therefore, have been observed in the SPM samples, in practice, this degradation pathway appeared to have had

little or no effect on these lipids. For example, no photodegradation products of epi-brassicasterol and 24-methylenecholesterol could be identified in any of the SPM samples investigated, while only relatively small amounts of photooxidation products of palmitoleic acid could be detected in samples collected after 11 June 2012 (Fig. 4). Photooxidation of chlorophyll (based on CPPI calculations) (Cuny et al., 1999) was also relatively weak at 2 m, although it increased slightly with depth (Fig. 2), and the inefficiency of photodegradation processes on the SPM was particularly evident through the observation of relatively high values of the $C_{25:3}$(*E*)/IP_{25} ratio (Table 2). Interestingly, the very weak photodegradation state of palmitoleic acid and chlorophyll in the 2 m SPM samples from 30 May to 07 June coincides with the period of maximum release of algal material from the melting ice (Brown et al., 2016). Overall, our data suggest that, despite the low water temperature and irradiance under the ice, which could potentially have enhanced Type II photosensitized oxidation of algal components (Amiraux et al., 2016), the algal cells released by sea ice and which remained suspended in the near surface waters, were in a healthy state, and that these relatively unaggregated particles were largely unaffected by photooxidative damage. Indeed, in healthy cells, the greater part of the photo-excited chlorophyll singlet state is used in the fast photochemical reactions of photosynthesis. The very small amount of the longer live triplet state resulting from intercrossing system (ICS) (Knox and Dodge, 1985), which can generate $^1O_2$ by reaction with ground state oxygen ($^3O_2$) via Type II processes, is efficiently quenched by the photo-protective system of the cells (Foote, 1976). Such data and interpretations support the hypothesis of Riebesell et al. (1991), that growing cells released by sea ice remain unaggregated (i.e. mainly in suspension), thereby increasing their seeding potential. Interestingly, the release of ice algae in good healthy state in the course of melting provides a continuous food source for under-ice grazers.

Quantification of the oxidation products of palmitoleic acid also enabled us to estimate the role of autoxidation processes in the degradation of suspended algal material. Although some samples of SPM exhibited relatively high autoxidation percentages (values reaching 65%) (Fig. 4), those collected at 2 m between 30 May and 07 June (Fig. 4A) were only weakly affected by these processes, consistent with the SPM comprising nearly all (ca. 100%; Brown et al., 2016) of the recently deposited ice-derived POC at this time.

4.2. Sediment trap samples

At 5 m, the fluxes of IP_{25} (Table 3), epi-brassicasterol (Fig. 8A) and 24-methylenecholesterol (Fig. 8C) increased significantly on 02 June and remained relatively high until 05 June, suggesting the occurrence of intensified settling of aggregated sea ice algal material to the traps during this period. Interestingly, quantitative estimates of the percentage of ice-derived POC (within total POC) also increased considerably from 11–60% between 30 May and 03 June (Brown et al., 2016). Although increases of the fatty acid concentration (Fig. 6A) and chl *a* content (Fig. 5A) were also evident, this deposition event was less noticeable for these lipids compared to IP_{25} and the sterols, probably due to their well-known lower biotic (Atlas and Bartha, 1992) and abiotic (Rontani et al., 1998; Christodoulou et al., 2010) stability. The strong contribution of sea ice algae to the sediment trap material is further evidenced by the similarity in the values of the (phytol + oxidation products)/IP_{25} ratio (ranging from 300–635 g/g) with those determined previously for the bottom (0–3 cm) sections of the corresponding sea ice cores (ranging from 45–750 g/g) (Rontani et al., 2014). However, in contrast to the SPM samples, very high proportions of oxidation products of epi-brassicasterol and 24-methylenecholesterol were also detected in the 5 m sediment trap samples (Fig. 8A and C) indicating that the sea ice algae in these sinking particles had undergone a strong degree of photooxidation state prior to deposition. In addition, the extent

of photodegradation was greater for 24-methylenecholesterol (mainly derived from diatoms, Volkman, 1986, 2003; Rampen et al., 2010) compared to epi-brassicasterol (arising from diatoms and/or prymnesiophytes, Volkman 1986, 2003), consistent with similar observations in the corresponding sea ice samples (Rontani et al., 2014) and in particles from the Beaufort Sea (Rontani et al., 2012). This difference in photoreactivity between the two sterols was previously attributed to a higher content of mycosporine-like amino acids that are known to protect cells from reactive oxygen species such as $^1O_2$ (Suh et al., 2003) in prymnesiophytes (Elliott et al., 2015). The very strong oxidation state of deposited sea ice algal material was further evidenced by the very low values of the $C_{25:3}$(*E*)/IP_{25} ratio (Table 3), the strong photooxidation state of chlorophyll (Fig. 5B) and relatively high proportions of the oxidation products of palmitoleic acid (Fig. 7A). Identification and quantification of the latter also enabled us to demonstrate that the degradation of these sinking particles mainly involved photooxidation, with only a minor contribution from autoxidation (Fig. 7A). Previously, Riebesell et al. (1991) suggested that less metabolically active sea ice algae were generally concentrated in aggregates, so we believe that the strong photooxidation state of the sediment trap material likely reflects a high contribution of aggregated senescent sea ice algae that sinks relatively slowly within the euphotic zone. Indeed, in dead cells or phytodetritus, there would be a shutdown of photosynthesis, such that an enhancement in the formation of excited chlorophyll (triplet) and $^1O_2$ (exceeding the quenching capacity of the photoprotective system) would be expected (Nelson, 1993).

A further increase of the fluxes of IP_{25}, epi-brassicasterol, 24-methylenecholesterol, chl *a* and fatty acids occurred at 5 m towards the end of sampling between 17 June and 23 June (Table 3, Figs. 5A, 6A and 8A and C). In these samples, chlorophyll (Fig. 5A), epi-brassicasterol (Fig. 8A) and 24-methylenecholesterol (Fig. 8C) were only weakly photodegraded, and significant photodegradation (ca. 50%) was only observed for palmitoleic

acid (Fig. 7A). These differences of photoreactivity are consistent with the involvement of steric hindrance during the attack of the sterol Δ^5 double bond by $^1O_2$ (Beutner et al., 2000) and the contrasting sensitivity of these constituents towards photodegradation processes at low temperature and irradiance (Amiraux et al., 2016). Indeed, during in vitro experiments carried out on senescent cells of the centric diatom *Chaetoceros neogracilis*, it was recently demonstrated that Type II photosensitized oxidation of palmitoleic acid was strongly enhanced by low temperatures and irradiances, while the opposite was true for the photodegradation of chl *a*. The strong increase of the (phytol + oxidation products)/IP_{25} ratio during this later stage of sampling (values ranging from 2505–4353 g/g) suggests that the deposited material corresponded to a combination of partially degraded sea ice algae supplemented by pelagic algae in a healthy state. Similarly, Brown et al. (2016) reported that the proportion of ice-derived POC decreased from 28 to 13% at 5 m over the same period. However, since the sampling site remained ice-covered throughout the study (ice thickness > 90 cm), we attribute this transition to an under-ice bloom (see Galindo et al., 2014; Mundy et al., 2014).

At 30 m, although the (phytol + oxidation products)/IP_{25} ratios (292 ± 138 g/g) were still relatively close to those observed previously in the bottom ice samples (see above), the fluxes of IP_{25} were higher than at 5 m (Table 3) indicating an even higher contribution of strongly aggregated sea ice algae to the material collected. However, in contrast to the 5 m samples, the $C_{25:3}$(*E*)/IP_{25} ratio in the 30 m sediment traps was consistently close to that measured in sea ice algae (Belt et al., 2013), while chlorophyll (Fig. 5D), epi-brassicasterol (Fig. 8B) and 24-methylcholesterol (Fig. 8D) were only weakly photodegraded, with only the very reactive palmitoleic acid exhibiting a degree of photodegradation similar to that seen in the samples collected at 5 m and towards the end of sampling (Fig. 7B). As such, we attribute the relative abiotic preservation of the material analyzed in the 30 m sediment traps to a high

497 contribution of highly aggregated senescent sea ice algae that settled rapidly out of the
498 euphotic zone (Lalande et al., 2016).

499 The enhanced concentrations of chlorophyll and palmitoleic acids in the 30 m trap
500 compared to the upper trap at 5 m probably results from their relatively higher abiotic
501 preservation. In contrast, the highest amounts of saturated fatty acids (especially palmitic
502 acid) at 30 m likely results from the presence of additional material derived from zooplankton
503 at this depth. Consistent with this suggestion, we could also detect significant amounts of
504 $C_{20:\Delta 11}$ and $C_{22:\Delta 11}$ *n*-alkan-1-ols in some of the 30 m trap samples, which are typical of wax
505 esters found in the large herbivorous copepods *Calanus hyperboreus* and *C. glacialis* that
506 undergo diapause (Graeve et al., 1994).

507 Our combined lipid (parent and oxidation products) data can be represented by a 3-
508 component conceptual scheme (Fig. 9) and described as follows: Ice algae released to the
509 water column during ice melt either remain in suspension in the surface layer or are subject to
510 rapid sinking to greater depths (Carey, 1987). The material remaining in suspension is
511 composed mainly of unaggregated cells that are largely unstressed, despite the dramatic
512 change of salinity that results during ice melt (Riebesell et al., 1991). Due to their healthy
513 state, however, these cells may continue to grow in surface waters and are only weakly
514 affected by Type II photosensitized oxidation processes. In contrast, those cells that are
515 stressed as a result of the melt process occur in aggregates of varying sizes (Riebesell et al.,
516 1991), the smallest being subject to a high degree of photooxidation, in part, due to their
517 relatively slow sinking rate out of the euphotic zone. However, since unaggregated cells in the
518 near surface waters do not appear to undergo the same degradation, our data indicate that the
519 involvement of intense photooxidation requires the combination of four key parameters: an
520 advanced senescent state of the cells, long residence times in the euphotic zone, low
521 temperature, and low irradiance (Amiraux et al., 2016). A significant part of this algal

material is also likely to undergo photodissolution before settling (Mayer et al. 2009). In contrast, the larger aggregates sink more rapidly out of the euphotic zone such that, despite their advanced senescent state, remain relatively preserved (unaffected by photodegradation) and likely contribute more strongly to the underlying sediments. As previously proposed by Riebesell et al. (1991), it seems that the process of aggregation acts as a mechanism for selection of cells less adapted to planktonic life.

5. Conclusions

By measuring various lipids and their characteristic oxidation products in suspended and sinking diatoms released from Arctic sea ice during a spring melt process, we have deduced that the nature and extent of degradation is quite variable, and is suggested to be attributable to the aggregation state of the cells and their physiological state. For example, suspended particles are mainly composed of growing cells with a high seeding potential for further growth, while metabolically less active cells are aggregated and concentrated in sinking particles. Due to their relatively slow sinking rate out of the euphotic zone and their advanced senescent state, the smallest aggregated sinking particles (collected at 5 m) are strongly photooxidized, while the larger aggregates (collected at 30 m) sink quickly out of the euphotic zone and remain relatively preserved. The very high photooxidation state of sinking particles collected at 5 m allowed us to confirm the strong efficiency of Type II photosensitized oxidation processes in senescent phytoplankton cells at low temperature and low irradiance previously observed in vitro.

Acknowledgements

This work was partially funded by the CNRS-INSU and the Aix-Marseille University. It was also funded by a Leverhulme Trust Research Project Grant, the University of

Plymouth, the Natural Sciences and Engineering Research Council of Canada (NSERC), Fonds de recherche du Québec—Nature et technologies (FRQNT), Canada Economic Development and the Polar Continental Shelf Program (PCSP) of Natural Resources Canada. The authors thank Christian Nozais for providing the sediment traps and Virginie Galindo, Mathew Gale, Marjolaine Blais and Joannie Charette for assistance in the field and/or the laboratory. This is a contribution to the research programs of ArcticNet, Québec-Océan, ISMER, Arctic Science Partnership (ASP) and the Canada Excellence Research Chair unit at the Centre for Earth Observation Science. We thank Dr. Sebastiaan Rampen and an anonymous reviewer for their useful and constructive comments.

Associate Editor–**Philip Meyers**

References

Amiraux, R., Jeanthon, C., Vaultier, F., Rontani, J.-F., 2016. Paradoxical effects of temperature and solar irradiance on the photodegradation state of killed phytoplankton. Journal of Phycology (in press).

Atlas, R.M., Bartha, R., 1992. Hydrocarbon biodegradation and oil spill bioremediation. In: Marshall, K.C. (Ed.), Advances in Microbial Ecology. Springer US, pp. 287–338.

Arrigo, K.R., Mock T., Lizotte M.P., Thomas D.N., Dieckmann G.S., 2010. Primary producers in sea ice. In: Thomas, D.N., Dieckmann, G.S. (Eds.), Sea Ice. 2nd ed. Wiley-Blackwell Publishing, Oxford, pp. 283–325.

Belt, S.T., Brown, T.A., Ringrose, A.E., Cabedo-Sanz, P., Mundy, C.J., Gosselin, M., Poulin, M., 2013. Quantitative measurement of the sea ice diatom biomarker IP_{25} and sterols in Arctic sea ice and underlying sediments: Further considerations for palaeo sea ice reconstruction. Organic Geochemistry 62, 33–45.

572 Belt, S.T., Müller, J., 2013. The Arctic sea ice biomarker IP_{25}: a review of current
573 understanding, recommendations for future research and applications in palaeo sea ice
574 reconstructions. Quaternary Science Reviews 79, 9–25.
575 Belt, S.T., Massé, G., Rowland, S.J., Poulin, M., Michel, C., LeBlanc, B., 2007. A novel
576 chemical fossil of palaeo sea ice: IP_{25}. Organic Geochemistry 38, 16–27.
577 Belt, S.T., Brown, T.A., Rodriguez, A.N., Sanz, P.C., Tonkin, A., Ingle, R., 2012. A
578 reproducible method for the extraction, identification and quantification of the Arctic
579 sea ice proxy IP_{25} from marine sediments. Analytical Methods 4, 705.
580 Beutner, S., Bloedorn, B., Hoffmann, T., Martin, H.-D., 2000. Synthetic singlet oxygen
581 quenchers. Methods in Enzymology, Elsevier, pp. 226–241.
582 Bowman, J.S., Rasmussen, S., Blom, N., Deming, J.W., Rysgaard, S., Sicheritz-Ponten, T.,
583 2012. Microbial community structure of Arctic multiyear sea ice and surface seawater
584 by 454 sequencing of the 16S RNA gene. ISME Journal 6, 11–20.
585 Brown, T.A., Belt, S.T., 2016. Novel tri- and tetra-unsaturated highly branched isoprenoid
586 (HBI) alkenes from the marine diatom *Pleurosigma intermedium*. Organic
587 Geochemistry 91, 120–122.
588 Brown, T.A., Belt, S.T., 2012a. Closely linked sea ice-pelagic coupling in the Amundsen Gulf
589 revealed by the sea ice diatom biomarker IP_{25}. Journal of Plankton Research 34, 647–
590 654.
591 Brown, T.A., Belt, S.T., 2012b. Identification of the sea ice diatom biomarker IP_{25} in Arctic
592 benthic macrofauna: direct evidence for a sea ice diatom diet in Arctic heterotrophs.
593 Polar Biology 35, 131–137.
594 Brown, T.A., Belt, S.T., Tatarek, A., Mundy, C.J., 2014. Source identification of the Arctic
595 sea ice proxy IP_{25}. Nature Communications 5. doi:10.1038/ncomms5197.

596 Brown, T.A., Belt, S.T., Gosselin, M., Levasseur, M., Poulin, M., Mundy, C.J., 2016.
597 Quantitative estimates of sinking sea ice particulate organic carbon based on the
598 biomarker IP_{25}. Marine Ecology Progress Series (in press).
599 Brown, T.A., Belt, S.T., Philippe, B., Mundy, C.J., Massé, G., Poulin, M., Gosselin, M., 2011.
600 Temporal and vertical variations of lipid biomarkers during a bottom ice diatom bloom
601 in the Canadian Beaufort Sea: further evidence for the use of the IP_{25} biomarker as a
602 proxy for spring Arctic sea ice. Polar Biology 34, 1857–1868.
603 Carey, A.G., Boudrias, M.A., 1987. Feeding ecology of *Pseudalibrotus* (=*Onisimus*) *litoralis*
604 Kröyer (Crustacea: Amphipoda) on the Beaufort Sea inner continental shelf. Polar
605 Biology 8, 29–33.
606 Caron, D.A., Gast, R.J., 2010. Heterotrophic protists associated with sea ice. In: Thomas,
607 D.N., Dieckmann, G.S. (Eds.), Sea Ice second ed., Wiley-Blackwell, Oxford, pp. 327–
608 356.
609 Christodoulou, S., Marty, J.-C., Miquel, J.-C., Volkman, J.K., Rontani, J.-F., 2009. Use of
610 lipids and their degradation products as biomarkers for carbon cycling in the
611 northwestern Mediterranean Sea. Marine Chemistry 113, 25–40.
612 Christodoulou, S., Joux, F., Marty, J.-C., Sempéré, R., Rontani, J.-F., 2010. Comparative
613 study of UV and visible light induced degradation of lipids in non-axenic senescent
614 cells of *Emiliania huxleyi*. Marine Chemistry 119, 139–152.
615 Cuny, P., Rontani, J.-F., 1999. On the widespread occurrence of 3-methylidene-7,11,15-
616 trimethylhexadecan-1,2-diol in the marine environment: a specific isoprenoid marker of
617 chlorophyll photodegradation. Marine Chemistry 65, 155–165.
618 Cuny, P., Romano, J.-C., Beker, B., Rontani, J.-F., 1999. Comparison of the photodegradation
619 rates of chlorophyll chlorin ring and phytol side chain in phytodetritus: is the phytyldiol

versus phytol ratio (CPPI) a new biogeochemical index? Journal of Experimental Marine Biology and Ecology 237, 271–290.

Curry, J.A., Schramm, J.L., Ebert, E.E., 1995. Sea ice-albedo climate feedback mechanism. Journal of Climate 8, 240–247.

Ehrenberg, B., Anderson, J.L., Foote, C.S., 1998. Kinetics and yield of singlet oxygen photosensitized by hypericin in organic and biological media. Photochemistry and Photobiology 68, 135–140.

Elliott, A., Mundy, C.J., Gosselin, M., Poulin, M., Campbell, K., Wang, F., 2015. Spring production of mycosporine-like amino acids and other UV-absorbing compounds in sea ice-associated algae communities in the Canadian Arctic. Marine Ecology Progress Series 541, 91–104.

Estapa, M.L., Mayer, L.M., 2010. Photooxidation of particulate organic matter, carbon/oxygen stoichiometry and related photoreactions. Marine Chemistry 122, 138–147.

Ewert, M., Deming, J.W., 2013. Sea ice microorganisms: Environmental constraints and extracellular responses. Biology (Basel) 2, 603–628.

Fahl, K., Kattner, G., 1993. Lipid content and fatty acid composition of algal communities in sea-ice and water from the Weddell Sea (Antarctica). Polar Biology 13, 405–409.

Ferrari, R., Jansen, M.F., Adkins, J.F., Burke, A., Stewart, A.L., Thompson, A.F., 2014. Antarctic sea ice control on ocean circulation in present and glacial climates. Proceedings of the National Academy of Science 111, 8753–8758.

Foote, C.S., 1976. Photosensitized oxidation and singlet oxygen: consequences in biological systems. In: Pryor, W.A. (Ed.), Free Radicals in Biology. Academic Press, New York, pp. 85–133.

644 Fortier, M., Fortier, L., Michel, C., Legendre, L., 2002. Climatic and biological forcing of the
645 vertical flux of biogenic particles under seasonal Arctic sea ice. Marine Ecology
646 Progress Series 225, 1–16.
647 Frankel, E.N., 1998. Lipid Oxidation. The Oily Press, Dundee.
648 Frankel, E.N., Neff, W.E., Bessler, T.R., 1979. Analysis of autoxidized fats by gas
649 chromatography–mass spectrometry: V. Photosensitized oxidation. Lipids 14, 961–967.
650 Galindo, V., Levasseur, M., Scarratt, M., Mundy, C., Gosselin, M., Kiene, R., Gourdal, M.,
651 Lizotte, M., 2015. Under-ice microbial dimethylsulfoniopropionate metabolism during
652 the melt period in the Canadian Arctic Archipelago. Marine Ecology Progress Series
653 524, 39–53.
654 Galindo, V., Levasseur, M., Mundy, C.J., Gosselin, M., Tremblay, J.-É., Scarratt, M., Gratton,
655 Y., Papakiriakou, T., Poulin, M., Lizotte, M., 2014. Biological and physical processes
656 influencing sea ice, under-ice algae, and dimethylsulfoniopropionate during spring in
657 the Canadian Arctic Archipelago. Journal of Geophysical Research: Oceans 119, 3746–
658 3766.
659 Girotti, A.W., 1998. Lipid hydroperoxide generation, turnover and effector action in
660 biological systems. Journal of Lipid Research 39, 1529–1542.
661 Gosselin, M., Levasseur, M., Wheeler, P.A., Horner, R.A., Booth, B.C., 1997. New
662 measurements of phytoplankton and ice algal production in the Arctic Ocean. Deep Sea
663 Research Part II: Topical Studies in Oceanography 44, 1623–1644.
664 Graeve, M., Kattner, G., Hagen, W., 1994. Diet-induced changes in the fatty acid composition
665 of Arctic herbivorous copepods, Journal of Experimental Marine Biology and Ecology
666 182, 97–110.
667 Hargrave, B.T., Walsh, I.D., Murray, D.W., 2002. Seasonal and spatial patterns in mass and
668 organic matter sedimentation in the North Water. Deep Sea Research Part II: Topical

669 Studies in Oceanography, The International North Water Polynya Study 49, 5227–
670 5244.
671 Hartmann D.L., 1994. Global physical climatology. International Geophysics Series, Vol. 56.
672 Academic Press, 412 pp.
673 Horner, R., Ackley, S., Dieckmann, G., Gulliksen, B., Hoshiai, T., Legendre, L., Melnikov, I.,
674 Reeburgh, W., Spindler, M., Sullivan, C., 1992. Ecology of sea ice biota: 1. Habitat,
675 terminology, and methodology. Polar Biology 12. doi:10.1007/BF00243113.
676 Knox, J.P., Dodge, A.D., 1985. Singlet oxygen and plants. Phytochemistry 24, 889–896.
677 Kulig, M.J., Smith, L.L., 1973. Sterol metabolism. XXV. Cholesterol oxidation by singlet
678 molecular oxygen. The Journal of Organic Chemistry 38, 3639–3642.
679 Kessel, D., Smith, K., 1989. Photosensitization with derivatives of chlorophylls.
680 Photochemistry and Photobiology 49, 157–160.
681 Lalande, C., Nöthig, E.-M., Bauerfeind, E., Hardge, K., Beszczynska-Möller, A., Fahl, K.,
682 2016. Lateral supply and downward export of particulate matter from upper waters to
683 the seafloor in the deep eastern Fram Strait. Deep-Sea Research I 114, 78–89.
684 Legendre, L., Ackley, S.F., Dieckmann, G.S., Gulliksen, B. Homer, R., Hoshiai, T.,
685 Melnikov, I.A., Reeburgh, W.S., Spindler, M., Sullivan, C.W., 1992. Ecology of sea ice
686 biota. 2. Global significance. Polar Biology 12, 429–444.
687 Leu, E., Wiktor, J.M., Søreide, J.E., Berge, J., Falk-Petersen, S., 2010. Fatty acid
688 composition, element concentration and isotope ratios of sea ice algae sampled in
689 Rijpfjorden, Svalbard, supplement to: Leu, Eva; Wiktor, Jozef M; Søreide, Janne E;
690 Berge, J; Falk-Petersen, Stig (2010): Increased irradiance reduces food quality of sea
691 ice algae. Marine Ecology Progress Series 411, 49–60.

692 Ligowski, R., Godlewski, M., Lukowski, A., 1992. Sea ice diatoms and ice edge planktonic
693 diatoms at the northern limit of the Weddell Sea pack ice. Proceedings of the NIPR
694 Symposium on Polar Biology 5, 9–20.
695 Marchand, D., Rontani, J.-F., 2001. Characterisation of photo-oxidation and autoxidation
696 products of phytoplanktonic monounsaturated fatty acids in marine particulate matter
697 and recent sediments. Organic Geochemistry 32, 287–304.
698 Mayer, L.M., Schick, L.L., Hardy, R., Estapa, M.L., 2009. Photodissolution and other
699 photochemical changes upon irradiation of algal detritus. Limnology and
700 Oceanography 54, 1688–1698.
701 Merzlyak, M.N., Hendry, G.A.F., 1994. Free radical metabolism, pigment degradation and
702 lipid peroxidation in leaves during senescence. Proceedings of the Royal Society of
703 Edinburgh B 102, 459–471.
704 Michel, C., Ingram, R.G., Harris, L.R., 2006. Variability in oceanographic and ecological
705 processes in the Canadian Arctic Archipelago. Progress in Oceanography 71, 379–401.
706 Michel, C., Nielsen, T., Nozais, C., Gosselin, M., 2002. Significance of sedimentation and
707 grazing by ice micro- and meiofauna for carbon cycling in annual sea ice (northern
708 Baffin Bay). Aquatic Microbial Ecology 30, 57–68.
709 Mundy, C., Gosselin, M., Gratton, Y., Brown, K., Galindo, V., Campbell, K., Levasseur, M.,
710 Barber, D., Papakyriakou, T., Bélanger, S., 2014. Role of environmental factors on
711 phytoplankton bloom initiation under landfast sea ice in Resolute Passage, Canada.
712 Marine Ecology Progress Series 497, 39–49.
713 Nelson, J.R., 1993. Rates and possible mechanism of light-dependent degradation of pigments
714 in detritus derived from phytoplankton. Journal of Marine Research 51, 155–179.

715 Nozais, C., Gosselin, M., Michel, C., Tita, G., 2001. Abundance, biomass, composition and
716 grazing impact of the sea-ice meiofauna in the North Water, northern Baffin Bay.
717 Marine Ecology Progress Series 217, 235–250.
718 Parsons, T.R., Maita, Y., Lalli, C.M., 1984. A Manual of Chemical and Biological Methods
719 for Seawater Analysis. Pergamon Press, Pons Point, NSW, Australia.
720 Porter, N.A., Caldwell, S.E., Mills, K.A., 1995. Mechanisms of free radical oxidation of
721 unsaturated lipids. Lipids 30, 277–290.
722 Ralph, P.J., Ryan, K.G., Martin, A., Fenton, G., 2007. Melting out of sea ice causes greater
723 photosynthetic stress in algae than freezing in. Journal of Phycology 43, 948–956.
724 Rampen, S.W., Abbas, B.A., Schouten, S., Sinninghe Damsté, J.S., 2010. A comprehensive
725 study of sterols in marine diatoms (Bacillariophyta): implications for their use as
726 tracers for diatom productivity. Limnology and Oceanography 55, 91–105
727 Renaud, P.E., Morata, N., Ambrose Jr., W.G., Bowie, J.J., Chiuchiolo, A., 2007. Carbon
728 cycling by seafloor communities on the eastern Beaufort Sea shelf. Journal of
729 Experimental Marine Biology and Ecology 349, 248–260.
730 Riebesell, U., Schloss, I., Smetacek, V., 1991. Aggregation of algae released from melting sea
731 ice -implications for seeding and sedimentation. Polar Biology 11, 239–248.
732 Rontani, J.-F., 2008. Photooxidative and autoxidative degradation of lipid components during
733 the senescence of phototrophic organisms. In: Matsumoto, T. (Ed.), Phytochemistry
734 Research Progress. Nova Science Publishers, pp. 115–154.
735 Rontani, J.-F., 2012. Photo- and free radical-mediated oxidation of lipid components during
736 the senescence of phototrophic organisms. In: Nagata, T. (Ed.), Senescence. Intech,
737 Rijeka, pp. 3–31.
738 Rontani, J.-F., Marchand, D., 2000. Photoproducts of phytoplanktonic sterols: a potential
739 source of hydroperoxides in marine sediments? Organic Geochemistry 31, 169–180.

Rontani, J.-F., Aubert, C., 2005. Characterization of isomeric allylic diols resulting from chlorophyll phytyl side-chain photo- and autoxidation by electron ionization gas chromatography/mass spectrometry. Rapid Communications in Mass Spectrometry 19, 637–646.

Rontani, J.-F., Raphel, D., Cuny, P., 1996. Early diagenesis of the intact and photooxidized chlorophyll phytyl chain in a recent temperate sediment. Organic Geochemistry 24, 825–832.

Rontani, J.-F., Cuny, P., Grossi, V., 1998. Identification of a "pool" of lipid photoproducts in senescent phytoplanktonic cells. Organic Geochemistry 29, 1215–1225.

Rontani, J.-F., Zabeti, N., Wakeham, S.G., 2009. The fate of marine lipids: Biotic vs. abiotic degradation of particulate sterols and alkenones in the Northwestern Mediterranean Sea. Marine Chemistry 113, 9–18.

Rontani, J.-F., Grossi, V., Faure, R., Aubert, C., 1994. "Bound" 3-methylidene-7,11,15-trimethylhexadecan-1,2-diol: a new isoprenoid marker for the photodegradation of chlorophyll-a in seawater. Organic Geochemistry 21, 135–142.

Rontani, J.F., Rabourdin, A., Marchand, D., Aubert, C., 2003. Photochemical oxidation and autoxidation of chlorophyll phytyl side chain in senescent phytoplanktonic cells: Potential sources of several acyclic isoprenoid compounds in the marine environment. Lipids 38, 241–254.

Rontani, J.-F., Belt, S.T., Vaultier, F., Brown, T.A., 2011. Visible light induced photo-oxidation of highly branched isoprenoid (HBI) alkenes: Significant dependence on the number and nature of double bonds. Organic Geochemistry 42, 812–822.

Rontani, J.-F., Belt, S.T., Brown, T.A., Vaultier, F., Mundy, C.J., 2014. Sequential photo- and autoxidation of diatom lipids in Arctic sea ice. Organic Geochemistry 77, 59–71.

764 Rontani, J.-F, Rabourdin, A., Pinot, F., Kandel, S., Aubert, C., 2005. Visible light-induced
765 oxidation of unsaturated components of cutins: a significant process during the
766 senescence of higher plants. Phytochemistry 66, 313–321.
767 Rontani, J.-F., Charriere, B., Forest, A., Heussner, S., Vaultier, F., Petit, M., Delsaut, N.,
768 Fortier, L., Sempéré, R., 2012. Intense photooxidative degradation of planktonic and
769 bacterial lipids in sinking particles collected with sediment traps across the Canadian
770 Beaufort Shelf (Arctic Ocean). Biogeosciences 9, 4787–4802.
771 Różańska, M., Gosselin, M., Poulin, M., Wiktor, J., Michel, C., 2009. Influence of
772 environmental factors on the development of bottom ice protist communities during the
773 winter–spring transition. Marine Ecology Progress Series 386, 43–59.
774 Smith, L.L., 1981. Cholesterol Autoxidation. Springer Science & Business Media.
775 Suh, H.-J., Lee, H.-W., Jung, J., 2003. Mycosporine glycine protects biological systems
776 against photodynamic damage by quenching singlet oxygen with a high efficiency.
777 Photochemistry and Photobiology 78, 109–113.
778 Suwa, K., Kimura, T., Schaap, A.P., 1977. Reactivity of singlet molecular oxygen with
779 cholesterol in a phospholipidic membrane matrix: a model for oxidative damage of
780 membranes. Biochemistry and Biophysical Research Communications 75, 785-792.
781 Tedesco, M., Fettweis, X., 2012. 21st century projections of surface mass balance changes for
782 major drainage systems of the Greenland ice sheet. Environmental Research Letters 7,
783 045405. doi:10.1088/1748-9326/7/4/045405
784 Vancoppenolle, M., Meiners, K.M., Michel, C., Bopp, L., Brabant, F., Carnat, G., Delille, B.,
785 Lannuzel, D., Madec, G., Moreau, S., Tison, J.-L., van der Merwe, P., 2013. Role of
786 sea ice in global biogeochemical cycles: emerging views and challenges. Quaternary
787 Science Reviews, 79, 207–230.

788 Volkman, J.K., 1986. A review of sterol markers for marine and terrigenous organic matter.
789 Organic Geochemistry 9, 83–99.
790 Volkman, J.K., 2003. Sterols in microorganisms. Applied Microbiology and Biotechnology
791 60, 495–506.
792 Volkman, J.K., 2005. Sterols and other triterpenoids: source specificity and evolution of
793 biosynthetic pathways. Organic Geochemistry 36, 139–159.
794 Zafiriou, O.C., Joussot-Dubien, J., Zepp, R.G., Zika, R.G., 1984. Photochemistry of natural
795 waters. Environmental Science and Technology 18, 358–371.
796

FIGURE CAPTIONS

Fig. 1. Structures and potential applications of the different lipid tracers of degradation processes used in the present work. [1]Hydroperoxides were quantified after $NaBH_4$-reduction to the corresponding alcohols.

Fig. 2. Estimates of chlorophyll *a* photooxidation in suspended particles collected at 2 m (A), 5 m (B) and 10 m (C).

Fig. 3. Fatty acid concentrations in suspended particles collected at 2 m (A), 5 m (B) and 10 m (C).

Fig. 4. Photo- and autoxidation percentages in suspended particles collected at 2 m (A), 5 m (B) and 10 m (C).

Fig. 5. Estimates of fluxes of chlorophyll *a* and chlorophyll photooxidation in sediment traps at 5 m (A and B) and at 30 m (C and D).

Fig. 6. Fluxes of fatty acids in sediment traps at 5 m (A) and 30 m (B).

Fig. 7. Photo- and autoxidation percentages of palmitoleic acid in sediment traps at 5 m (A) and 30 m (B).

Fig. 8. Fluxes of epi-brassicasterol and 24-methylenecholesterol and their photooxidation products in sediment traps at 5 m (A and C) and at 30 m (B and D).

822

823 **Fig. 9**. Three-component conceptual scheme summarizing the behavior of algae released to

824 the water column during ice melt in Resolute Bay (Canadian Arctic).

825

Figure 1

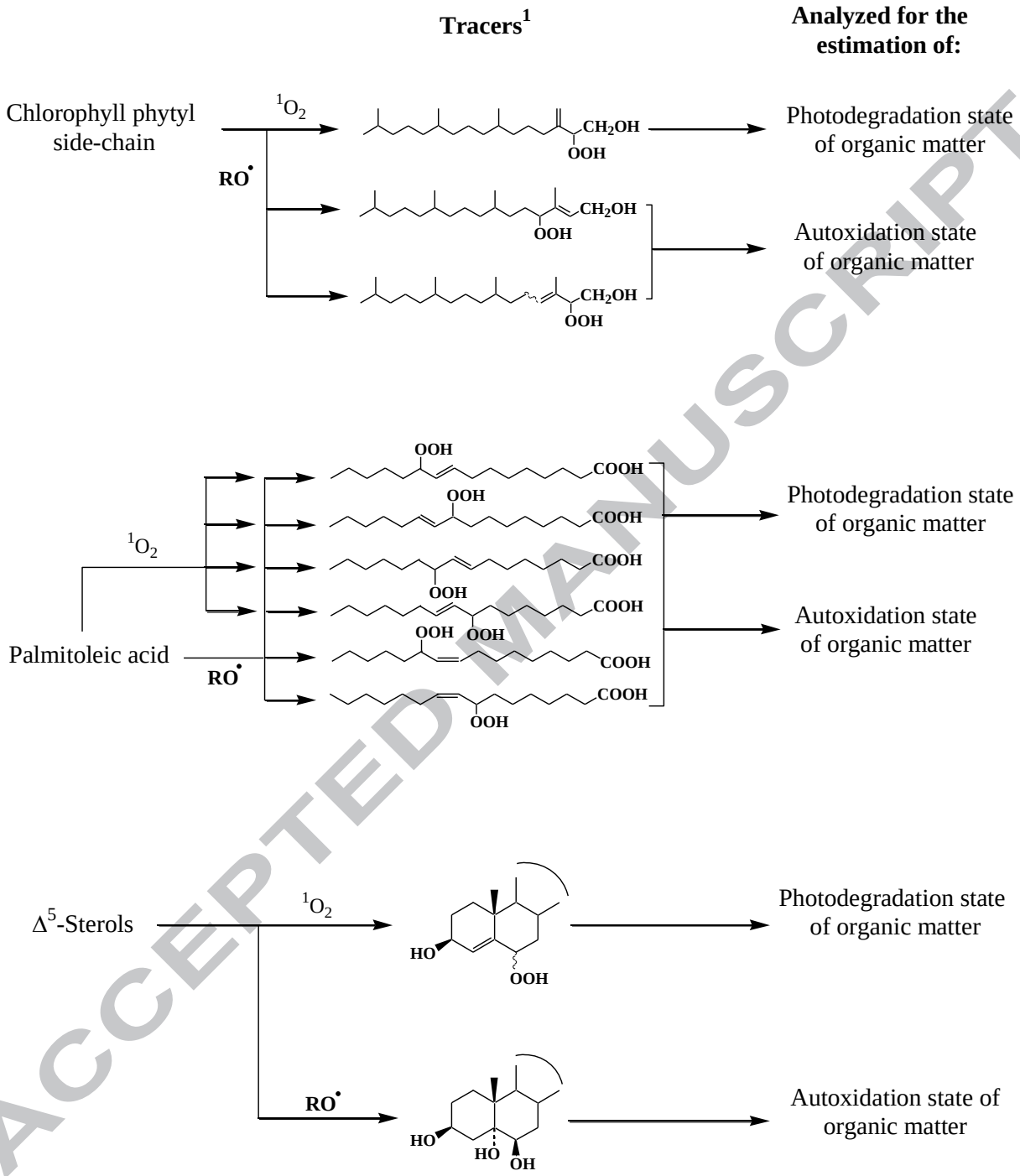

Figure 2

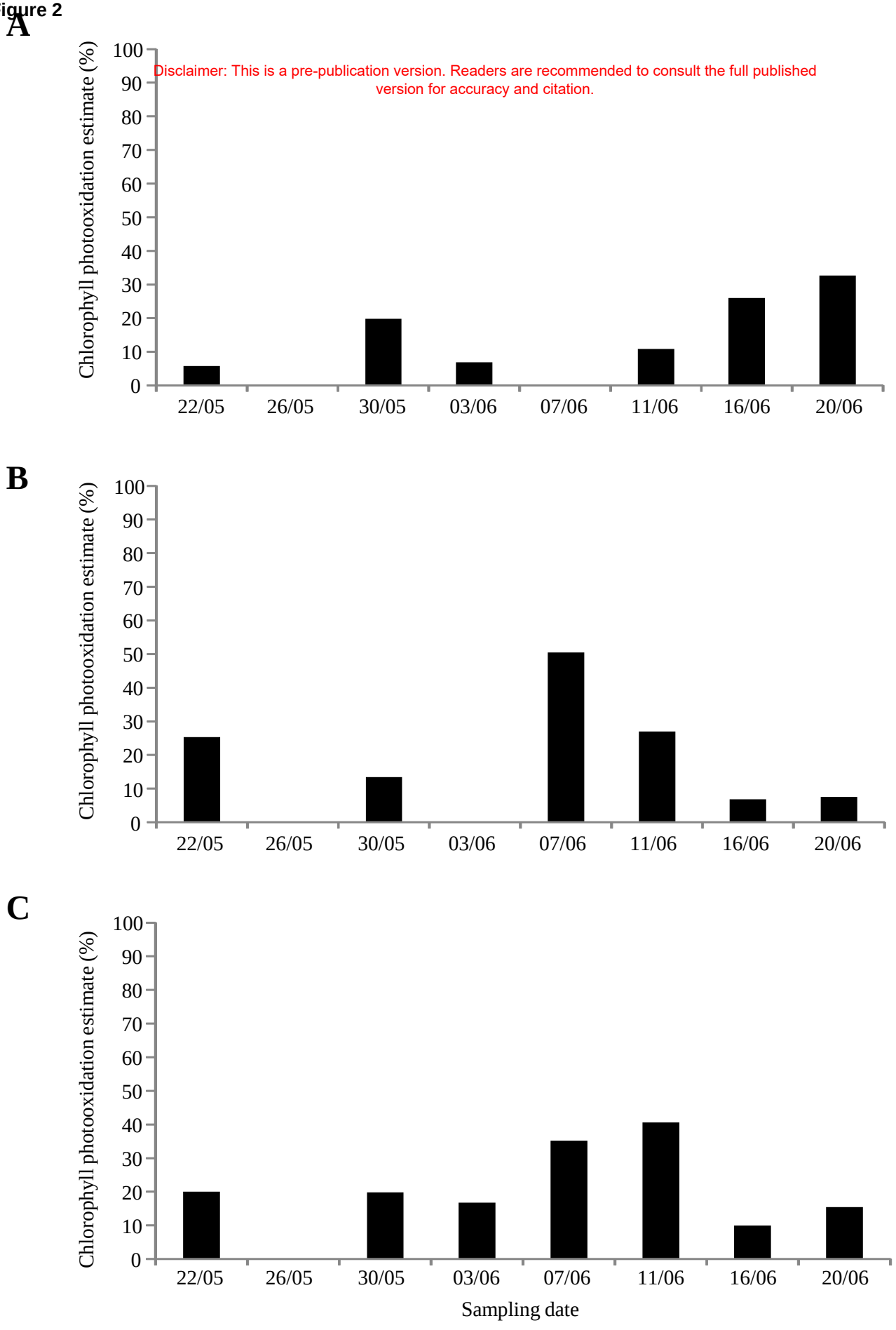

Figure 3

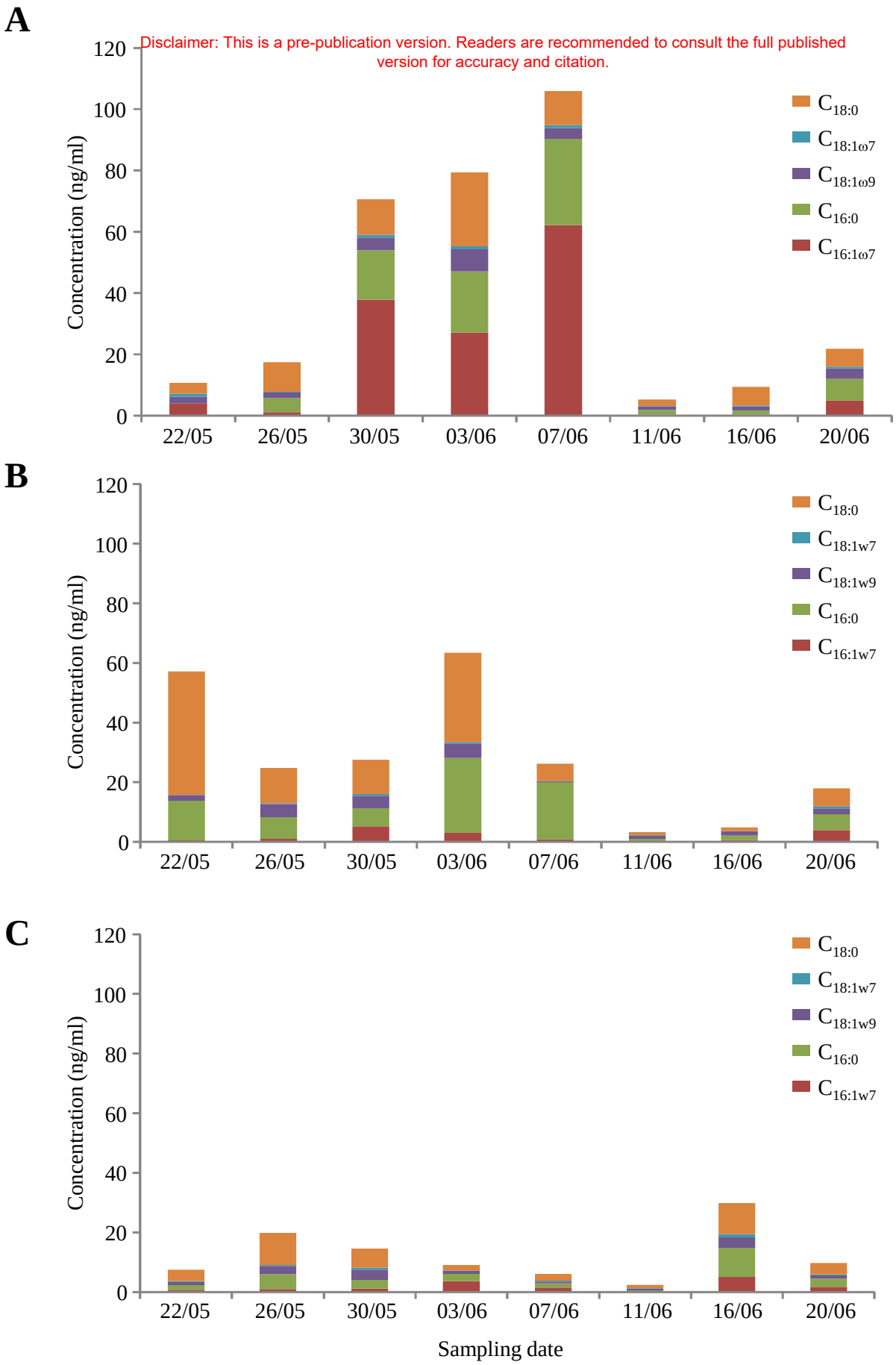
A
Disclaimer: This is a pre-publication version. Readers are recommended to consult the full published version for accuracy and citation.
Concentration (ng/ml)
120
100
80
60
40
20
0
22/05
26/05
30/05
03/06
07/06
11/06
16/06
20/06
C18:0
C18:1ω7
C18:1ω9
C16:0
C16:1ω7
B
Concentration (ng/ml)
C18:0
C18:1w7
C18:1w9
C16:0
C16:1w7
C
Concentration (ng/ml)
Sampling date

Figure 4

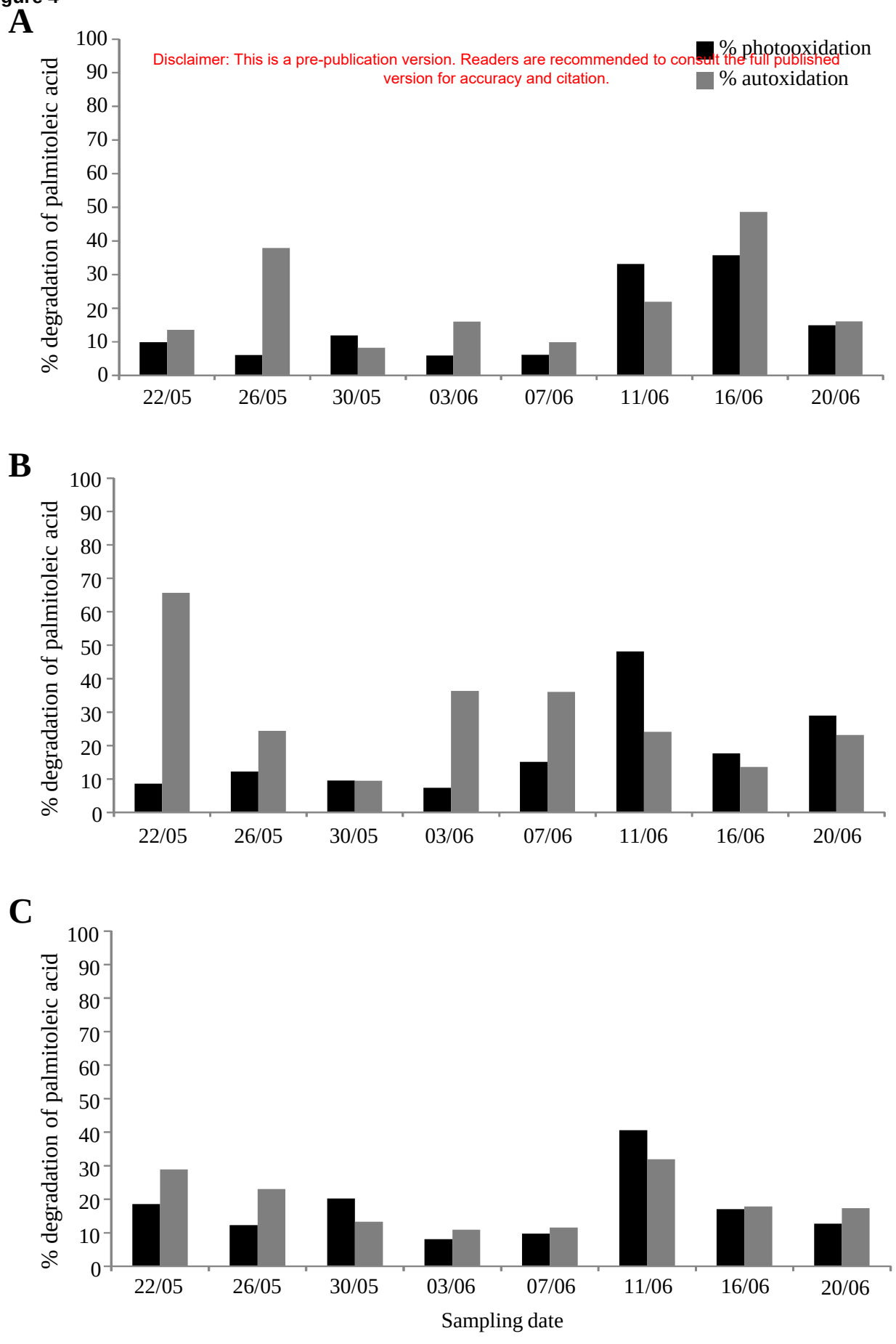

Figure 5

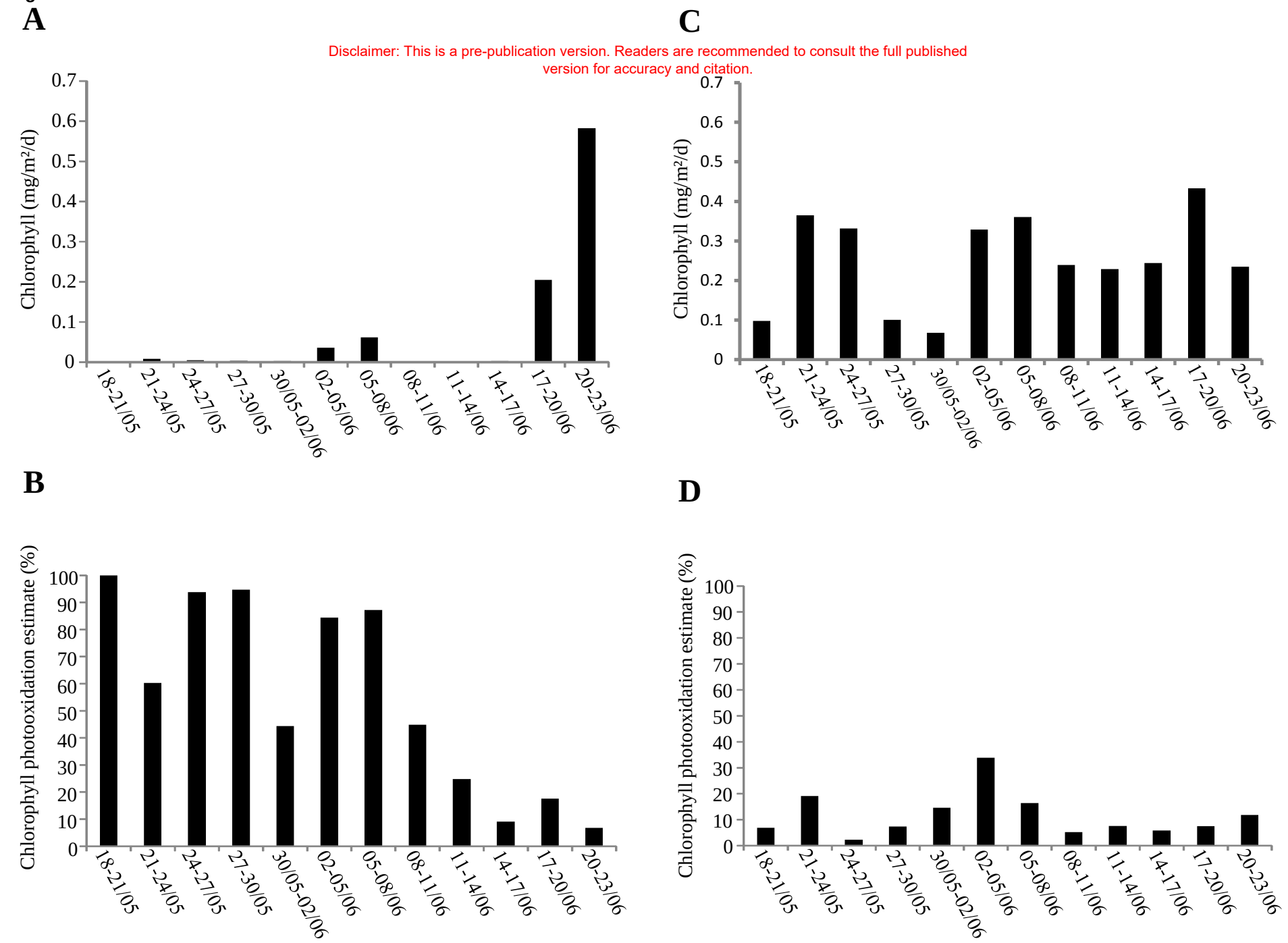

Figure 6

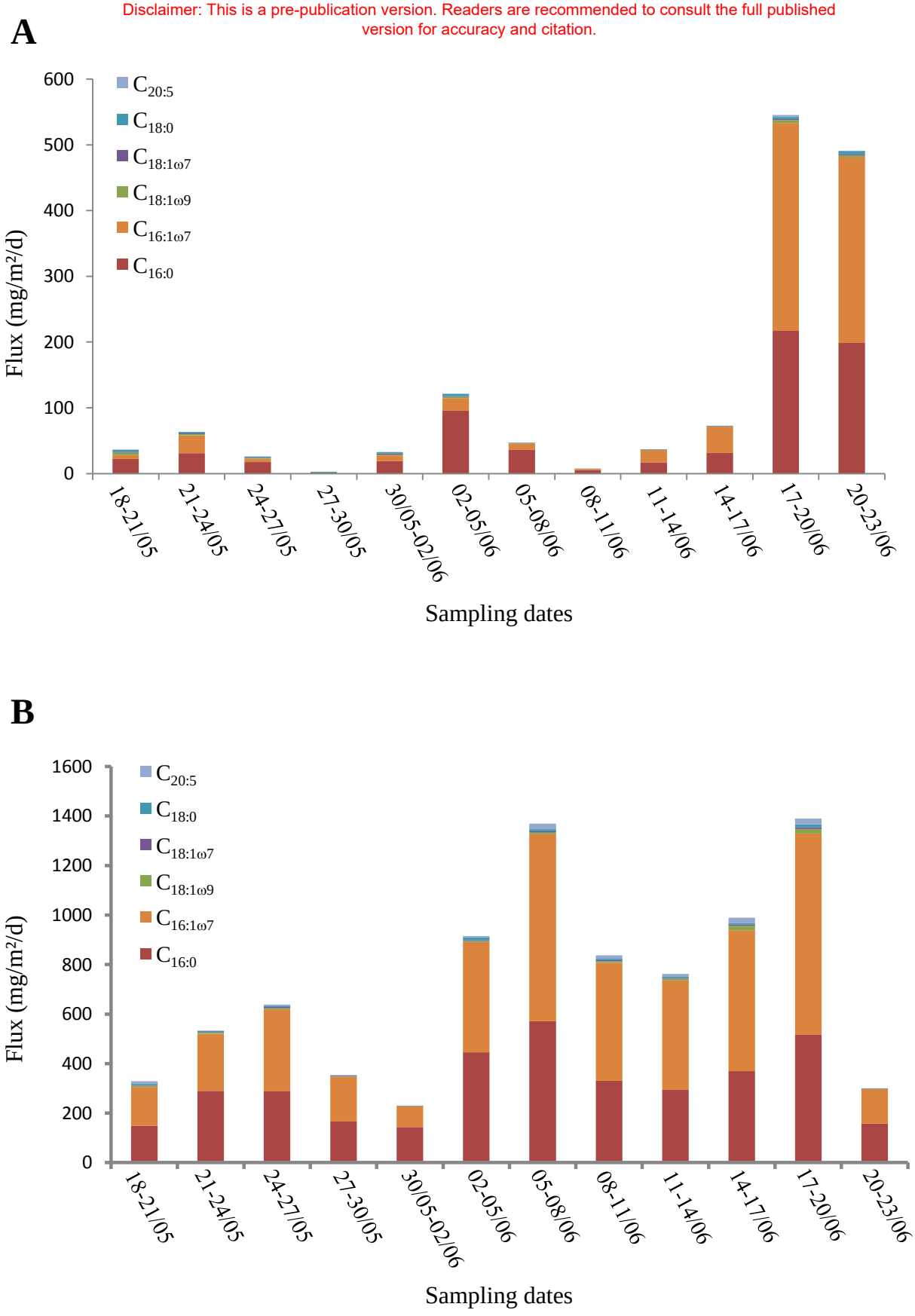

Figure 7

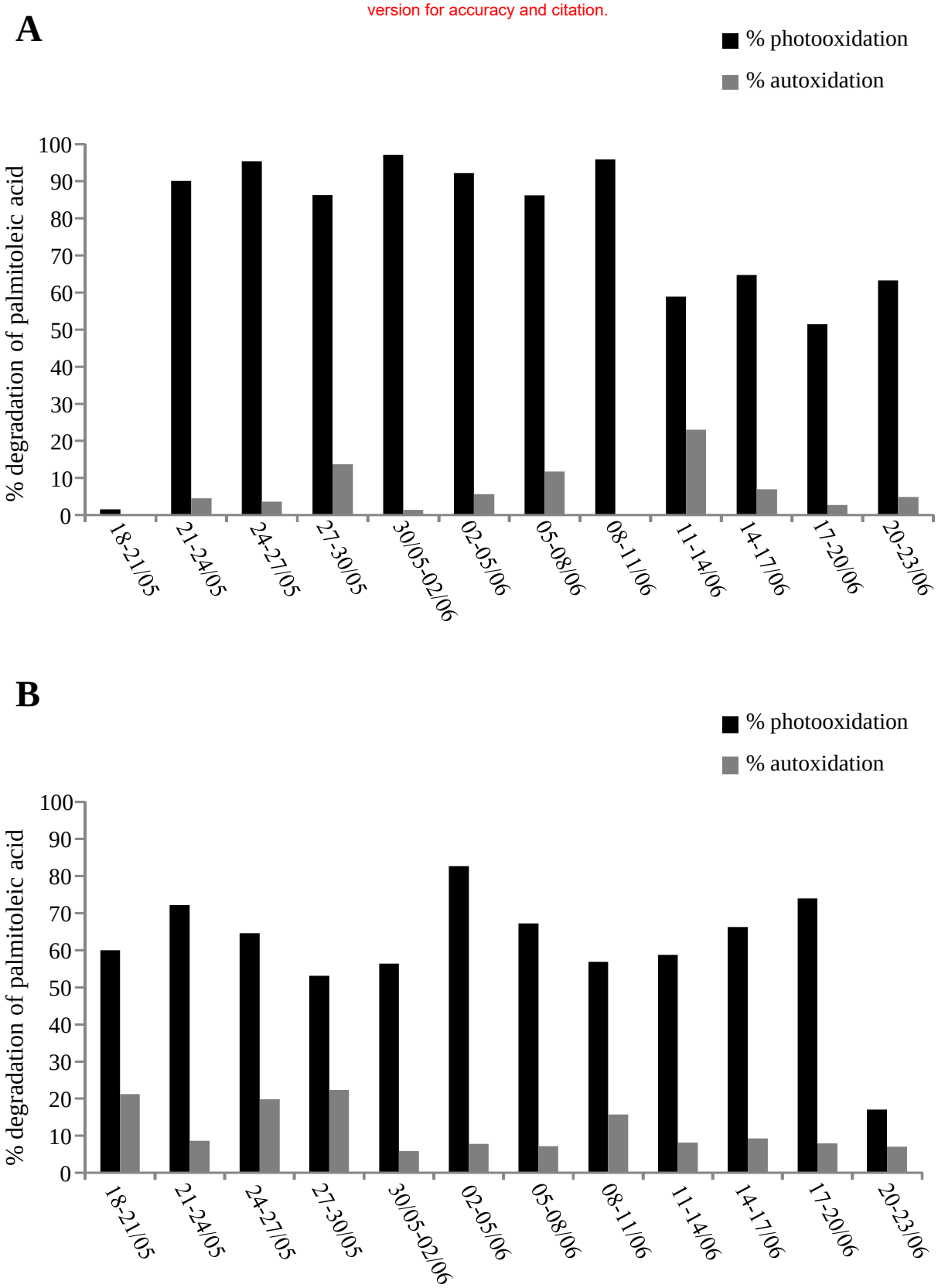

Figure 8

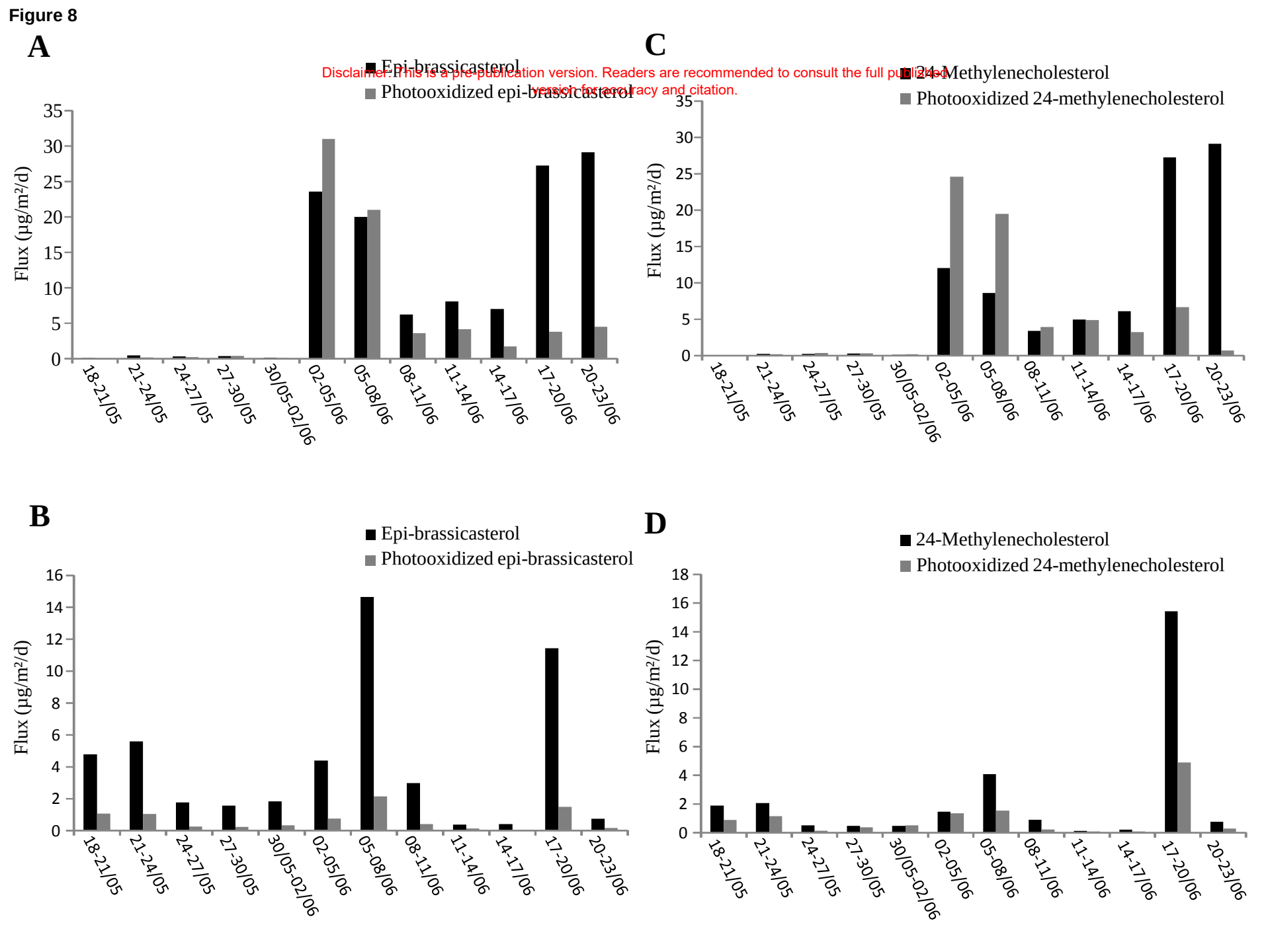

Figure 9

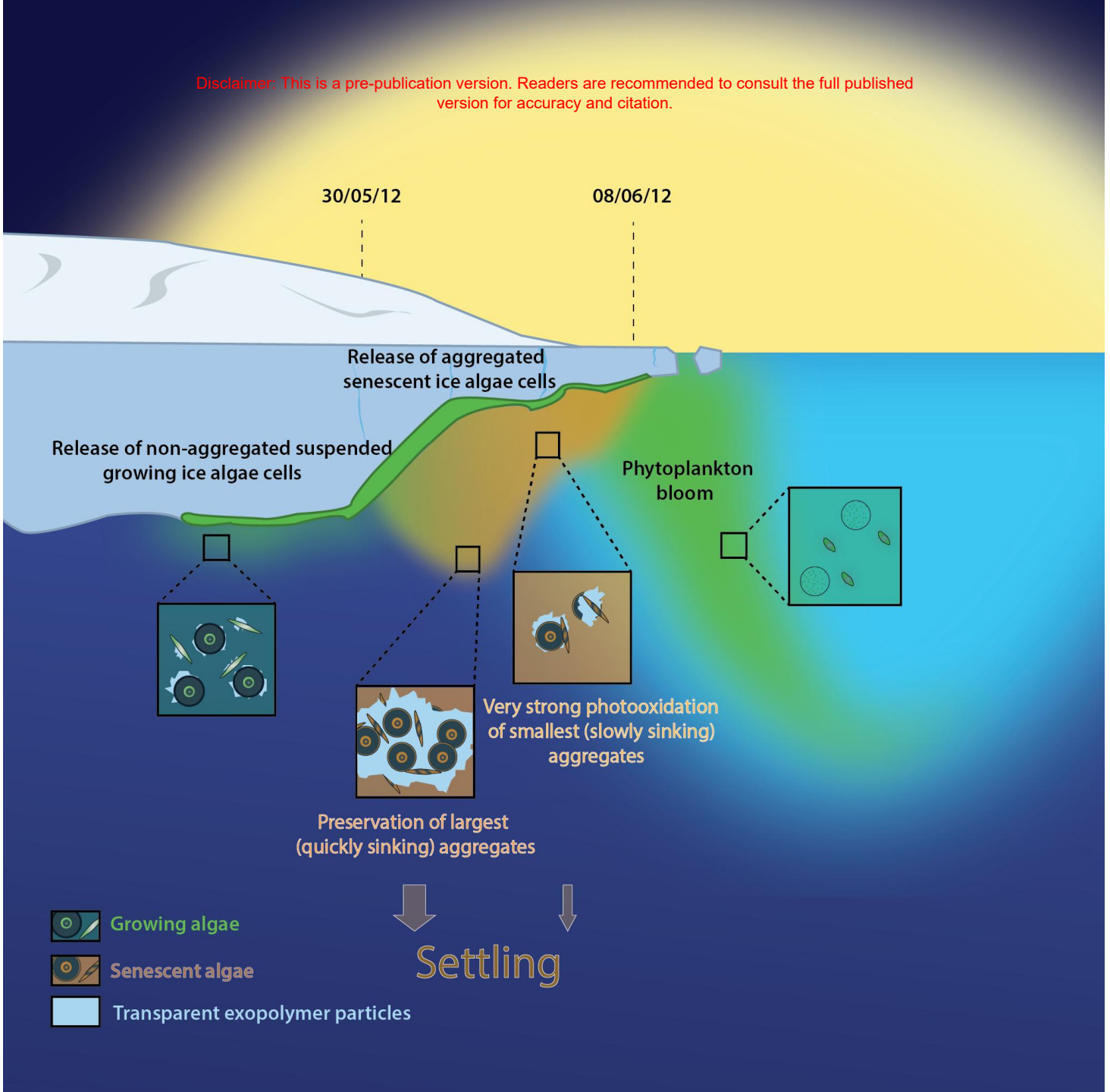
Disclaimer: This is a pre-publication version. Readers are recommended to consult the full published version for accuracy and citation.
30/05/12
08/06/12
Release of aggregated senescent ice algae cells
Release of non-aggregated suspended growing ice algae cells
Phytoplankton bloom
Very strong photooxidation of smallest (slowly sinking) aggregates
Preservation of largest (quickly sinking) aggregates
Growing algae
Senescent algae
Transparent exopolymer particles
Settling

826

827

828 **Table 1**

829 Concentrations (ng/ml) of chlorophyll-*a* and Δ^5-sterols in SPM samples.

830

Sampling dates	22/05/2012			26/05/2012			30/05/2012			03/06/2012			07/06/2012			11/06/2012			16/06/2012			20/06/2012		
Depth (m)	2	5	10	2	5	10	2	5	10	2	5	10	2	5	10	2	5	10	2	5	10	2	5	10
Chlorophyll *a*	0.36	0.35	0.30	0.34	0.15	0.39	0.65	0.17	0.22	0.54	0.42	0.26	0.17	0.43	0.41	0.65	0.70	0.38	0.22	0.31	0.18	0.48	0.37	0.44
Epi-brassicasterol	0.06	0.02	0.04	0.01	0.03	0.02	0.08	0.03	0.01	0.12	0.03	0.08	0.24	nd*	0.03	0.05	0.04	0.05	0.09	0.01	0.10	0.04	0.07	0.03
24-Methylenecholesterol	0.03	0.01	0.02	nd	0.01	0.01	0.04	0.02	0.01	0.04	0.01	0.03	0.15	nd	0.02	0.03	0.02	0.03	0.04	nd	0.05	0.01	0.02	0.01

831 * nd: not detected

832

Table 2

Concentrations of 2,6,10,14-tetramethyl-7-(3-methylpent-4-enyl)-pentadecane (IP_{25}) and 2,6,10,14-tetramethyl-7-(3-methylpenta-1,4-dienyl)-pentadeca-7(20*E*),9*E*-diene ($C_{25:3}$(*E*)) in the different SPM samples analyzed.

Sampling date	Depth (m)	IP_{25} (ng/ml)	$C_{25:3}$(*E*) ng/ml	$C_{25:3}$(*E*)/IP_{25}
22/05/2012	2	14.7	3.27	0.222
	5	7.4	2.67	0.361
	10	8.6	2.70	0.313
26/05/2012	2	13.0	2.59	0.200
	5	11.5	3.60	0.313
	10	12.7	3.37	0.265
30/05/2012	2	64.4	10.3	0.153
	5	2.1	0.84	0.400
	10	7.7	1.79	0.232
03/06/2012	2	19.7	5.94	0.301
	5	16.8	3.01	0.179
	10	15.5	2.69	0.173
07/06/2012	2	41.6	na[$]	
	5	17.6	na	
	10	17.5	na	
11/06/2012	2	7.0	nd*	0
	5	9.5	nd	0
	10	12.3	nd	0
16/06/2012	2	9.3	0.47	0.051
	5	14.6	nd	0
	10	14.6	nd	0
20/06/2012	2	30.3	nd	0
	5	15.7	nd	0
	10	15.6	nd	0
23/06/2012	2	12.6	nd	0
	5	13.1	nd	0
	10	14.1	nd	0

* nd: not detected (S/N > 3)

[$] na : not analyzed (contamination)

840 **Table 3**

841 Fluxes of 2,6,10,14-tetramethyl-7-(3-methylpent-4-enyl)-pentadecane (IP_{25}) and 2,6,10,14-
842 tetramethyl-7-(3-methylpenta-1,4-dienyl)-pentadeca-7(20*E*),9*E*-diene ($C_{25:3}$(*E*)) in the
843 different trap samples analyzed.

Sampling dates	Depth (m)	IP_{25} (ng/m^2/d)	$C_{25:3}$(*E*) (ng/m^2/d)	$C_{25:3}$(*E*)/IP_{25}
18-21/05/2012	5	1.10	nd*	0
	30	na[$]	na	
21-24/05/2012	5	2.25	nd	0
	30	na	na	
24-27/05/2012	5	1.67	nd	0
	30	5.51	1.03	0.187
27-30/05/2012	5	1.81	nd	0
	30	3.79	0.13	0.033
30/05-02/06/2012	5	1.30	nd	0
	30	2.68	0.28	0.103
02-05/06/2012	5	3.08	0.04	0.014
	30	6.77	1.02	0.151
05-08/06/2012	5	3.96	0.09	0.023
	30	7.59	1.40	0.184
08-11/06/2012	5	0.60	nd	0
	30	10.19	1.22	0.120
11-14/06/2012	5	1.43	nd	0
	30	5.37	0.96	0.180
14-17/06/2012	5	1.16	nd	0
	30	8.27	1.67	0.202
17-20/06/2012	5	2.44	0.16	0.065
	30	3.42	0.49	0.144
20-23/06/2012	5	4.38	0.54	0.124
	30	1.59	0.18	0.115

844 * nd: not detected (S/N > 3)
845 [$] na : not analyzed.
846

847 Lipid degradation products were analyzed in particles collected in the Arctic

848 Suspended particles appeared to be composed of unaggregated living cells

849 Photooxidation processes act strongly in slowly sinking aggregated cells

850 The larger aggregates sink quickly and escape photooxidation

851 Aggregation plays a key role in the degradation of sea ice algae

852